J Geod
DOI 10.1007/s00190-014-0786-9

ORIGINAL ARTICLE

Measurement of slow-moving along-track displacement from an efficient multiple-aperture SAR interferometry (MAI) stacking

Min-Jeong Jo · Hyung-Sup Jung · Joong-Sun Won · Michael P. Poland · Asta Miklius · Zhong Lu

Received: 15 August 2014 / Accepted: 20 December 2014

Abstract Multiple-aperture SAR interferometry (MAI) has demonstrated outstanding measurement accuracy of along-track displacement when compared to pixel-offset-tracking methods; however, measuring slow-moving (cm/year) surface displacement remains a challenge. Stacking of multi-temporal observations is a potential approach to reducing noise and increasing measurement accuracy, but it is difficult to achieve a significant improvement by applying traditional stacking methods to multi-temporal MAI interferograms. This paper proposes an efficient MAI stacking method, where multi-temporal forward- and backward-looking residual interferograms are individually stacked before the MAI interferogram is generated. We tested the performance of this method using ENVISAT data from Kīlauea Volcano, Hawai'i, where displacement on the order of several centimeters per year is common. By comparing results from the proposed stacking methods with displacements from GPS data, we documented measurement accuracies of about 1.03 and 1.07 cm/year for the descending and ascending tracks, respectively—an improvement of about a factor of two when compared with that from the conventional stacking approach. Three-dimensional surface-displacement maps can be constructed by combining stacked InSAR and MAI observations, which will contribute to a better understanding of a variety of geological phenomena.

Keywords Along-track displacement · SAR interferometry · MAI · Stacking · Kīlauea Volcano

M.-J. Jo · J.-S. Won
Department of Earth System Sciences, Yonsei University, Seoul 120-749, Republic of Korea
e-mail: owen009@yonsei.ac.kr

J.-S. Won
e-mail: jswon@yonsei.ac.kr

H.-S. Jung (✉)
Department of Geoinformatics, University of Seoul, 90 Jeonnong-dong, Dongdaemun-gu, Seoul 130-743, Republic of Korea
e-mail: hsjung@uos.ac.kr

M. P. Poland · A. Miklius
The U.S. Geological Survey, Hawaiian Volcano Observatory, Hawaii National Park, HI 96718-0051, USA
e-mail: mpoland@usgs.gov

A. Miklius
e-mail: asta@usgs.gov

Z. Lu
Department of Earth Sciences, Southern Methodist University, Dallas, TX 75275, USA
e-mail: zhonglu@mail.smu.edu

1 Introduction

Interferometric synthetic aperture radar (InSAR) is a powerful technique for measuring surface displacement (Massonnet et al. 1993; Amelung et al. 2007; Sandwell et al. 2008; Lu et al. 2010; Zhang et al. 2012), but its ability is limited to the radar line-of-sight (LOS) direction. Multiple aperture SAR interferometry (MAI), which can measure displacement in the along-track direction (perpendicular to the LOS direction), was proposed by Bechor and Zebker (2006) and improved by Jung et al. (2009) to overcome the limitations of conventional InSAR and can even be used to retrieve three-dimensional surface motion (Jung et al. 2011; Hu et al. 2012). The MAI method, which uses split-beam InSAR processing to create one forward- and one backward-looking interferogram and then constructs a multiple-aperture interferogram (designated an MAI interferogram within this paper) by subtracting the backward-looking interferogram from forward-looking interferogram, has achieved an improvement in measurement accuracy compared to other methods for measur-

Published online: 09 January 2015

ing along-track displacement, such as pixel offset tracking (Fialko et al. 2001; Jonsson et al. 2002).

The original MAI method had an along-track measurement accuracy of about 6.4 cm for ERS data (Bechor and Zebker 2006), which is about an order-of-magnitude coarser than the sub-centimeter accuracy of conventional LOS InSAR. For that reason, MAI has been used primarily for measuring large-scale displacement, such as that due to earthquakes, volcanic eruptions, or glacier movement (Jung et al. 2011, 2013b; Mcmillan et al. 2012). More recently, Jung et al. (2011) achieved an MAI accuracy of approximately 3.6 cm while using ALOS PALSAR imagery to measure along-track displacement during a dike emplacement event at Kīlauea Volcano, Hawai'i, in June 2007. Despite the enhancement in MAI performance, it is still challenging to measure surface displacements that are on the order of a few centimeters per year.

Multi-temporal InSAR (MTInSAR) approaches, which can be divided into stacking and time-series approaches, enable us to reduce noise in measuring surface displacements. Stacking is a simple and often-used method to improve the measurement accuracy of LOS displacements (Wright et al. 2001; Lyons and Sandwell 2003) because the procedure suppresses randomly distributed noise (due to atmospheric effects, for instance) and enables the identification of relatively small displacements. Time-series analysis has been widely used for the precise measurement of LOS displacements because it allows for a better separation of signal and noise compared to the stacking method (Ferretti et al. 2001; Berardino et al. 2002). In the case of non-random seasonal variations of the atmospheric signal, however, MTInSAR time-series methods can be biased due to uneven data sampling (Doin et al. 2009; Jo et al. 2010). Like the stacking approach for conventional interferograms, stacking of multi-temporal MAI observations can improve the resolution of along-track surface motion, which makes it possible to identify relatively small displacements. But what is the optimal approach for MAI stacking, and what levels of accuracy can be achieved?

We propose an efficient stacking method for multi-temporal MAI (MtMAI) observations that aims to improve measurement of slow-moving along-track surface displacements (on the order of a few centimeters per year). This stacking method is designed to maximize the coherence of sub-aperture interferograms. We demonstrate the performance of the proposed method using ascending and descending ENVISAT ASAR data from Kīlauea Volcano, Hawai'i, acquired during 2007–2010—a time period that includes along-track displacement rates on the order of several cm/year. Comparison of displacement velocities from our stacked MAI data with those from GPS confirms the high performance of the proposed stacking method. These data can be used to construct 3-D surface-displacement maps, thereby providing information to support a better understanding of a wide variety of geological phenomena. In addition, this stacking method can be extended to derive displacement time series for along-track surface motion—another key piece of information useful for interpretations of geologic processes.

This paper is organized as follows: Section 2 introduces the principles of MAI and explains the proposed MAI stacking algorithm in detail. Section 3 describes performance results of the proposed method from ENVISAT descending and ascending pairs. Discussion and Conclusions follow in Sect. 4.

2 Methodology

2.1 Brief introduction to the MAI technique

As defined by Bechor and Zebker (2006) and Jung et al. (2009), MAI utilizes sub-aperture single-look-complex (SLC) images (forward- and backward-looking) to measure along-track surface displacement. Four SLC images are constructed from two raw SAR scenes by modification of the Doppler Centroid, and then two pairs of interferograms are generated. Along-track surface displacements measured by MAI can be defined as Bechor and Zebker (2006)

$$\phi_{\mathrm{MAI}} = \phi_{\mathrm{f}} - \phi_{\mathrm{b}} = -\frac{4\pi}{l} n x, \tag{1}$$

where ϕ_{f} and ϕ_{b} are the forward- and backward-looking interferometric phases, respectively, l is the effective antenna length, x is the along-track surface displacement, and n is the fraction of the full-aperture beam width that is a normalized squint. From Eq. (1), the measurement sensitivity of MAI is primarily a function of the antenna length. In the case of half-aperture processing ($n = 0.5$), a phase change of 2π would be equivalent to 8.9 and 10 m of along-track displacement for ALOS and ERS/ENVISAT, respectively. The forward- and backward-looking interferometric phases are independent variables; therefore, the standard deviation of the MAI phase, $\sigma_{\varphi,\mathrm{MAI}}$, as given by Jung et al. (2009) [based on the previous definition by Rodriguez and Martin (1992)] is

$$\sigma_{\varphi,\mathrm{MAI}} \approx \frac{1}{\sqrt{N_{\mathrm{L}}}} \frac{\sqrt{1-\rho^2}}{\rho}, \tag{2}$$

where N_{L} is the number of looks to be averaged and ρ is the interferometric coherence (Zebker and Villasenor 1992). The standard deviation of the interferometric phase, in contrast, is a function of coherence, which is heavily influenced by the signal-to-noise ratio (SNR), spatial decorrelation due to the imaging geometry of the SAR, temporal decorrelation, and other effects (Zebker and Villasenor 1992). The standard deviation of the MAI phase can thus be represented in terms of uncertainties on the along-track displacement based on Eq. (1), which is

$$\sigma_{x,\mathrm{MAI}} = \frac{l}{4\pi \cdot n}\sigma_{\varphi,\mathrm{MAI}}, \tag{3}$$

where $\sigma_{x,\mathrm{MAI}}$ is the uncertainty in the along-track displacement.

2.2 A proposed MAI stacking algorithm

The accuracy of MAI displacement is a function of phase noise as well as phase distortions induced by differences in the perpendicular baseline between the forward- and backward-looking interferograms. Phase distortions induced by heterogeneous atmospheric conditions reduce the measurement accuracy of interferograms (Jo et al. 2010; Liu et al. 2014). In the case of MAI, atmospheric phase delays related to water vapor are removed by cancelation between the forward- and backward-looking interferograms (Bechor and Zebker 2006). The ionospheric effect, however, remains problematic. Stacking of multi-temporal MAI observations is one solution, along with other methods (Jung et al. 2013a; Liu et al. 2014), for minimizing noise in MAI-derived displacement measurements.

Like conventional InSAR stacking, conventional MAI stacking averages all available MAI interferograms.

$$v_{\mathrm{MAI}}(x) = \frac{l}{4\pi \cdot n}\sum_{i=1}^{N}\phi^{i}_{\mathrm{MAI}}(x) \Big/ \sum_{i=1}^{N}\Delta t^{i}, \tag{4}$$

where $v_{\mathrm{MAI}}(x)$ is the along-track velocity, N is the number of MAI interferograms, and ϕ^{i} and Δt^{i} are the phase value and time duration, respectively, of the ith MAI interferogram. A more rigorous approach can be carried out using the weighted least-squares solution (Simons and Rosen 2007). This method, however, did not show a significant improvement in resolution for along-track slow-moving surface displacement over individual MAI interferograms. In particular, conventional MAI stacking does not improve measurement ability in low-coherence regions. The accuracy of MAI depends largely on the phase noise of the forward- and backward-looking interferograms. This means that enhancing coherence of the forward- and backward-looking interferograms will lead to improvement of MAI measurement accuracy. Jung et al. (2009) found that filtering and multilooking of the individual forward- and backward-looking interferograms achieved better results than applying the same filtering and multilooking to the derived MAI interferogram because the coherence of the derived MAI interferogram is worse than that of the sub-aperture interferograms. Figure 1 shows a comparison between coherence values of MAI interferograms and those of forward- and backward-looking interferograms from a descending ENVISAT track over Kīlauea Volcano. The slope of dashed line between two values is 1, and it is clear that the coherence values of all measured points are higher for the forward- and backward-looking interferograms than for the derived MAI interferogram, especially at low levels of coherence. In addition, the MAI coherence level is improved when the sub-aperture interferograms that are used to make the MAI image have higher coherence values. A few points showing similar coherence from sub-aperture interferograms and MAI interferograms result from the boundaries between low and high coherence regions. These points are distributed mostly between coherence levels of 0.6 and 0.7, as seen in Fig. 1.

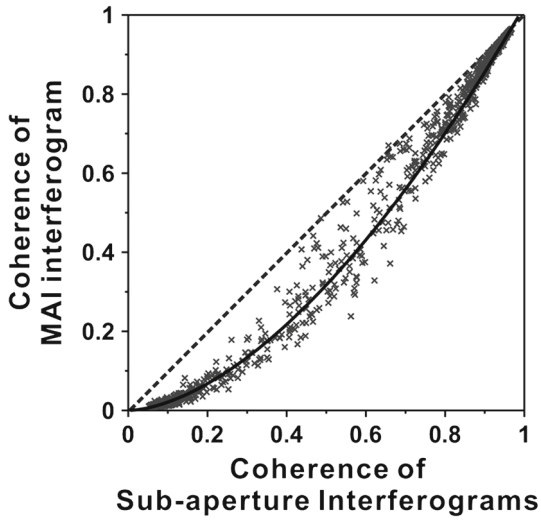

Fig. 1 Comparison of coherence values between MAI and sub-aperture (forward- and backward-looking) interferograms from descending-orbit data (track 429)

From this result, we presumed that the coherence level of MAI interferograms is closely related to the coherence levels of sub-aperture interferograms. It would be expected that the higher level of coherence for sub-aperture interferograms should lead to an improvement in the resolution of along-track displacements because the coherence value is crucial for determining the measurement accuracy of the MAI interferogram; thus, it is important to maximize the coherence of sub-aperture interferograms.

The core of the proposed stacking method for improving the resolution of MtMAI observations is to use the residual forward- and backward-looking interferograms for creating the MAI interferogram. Residual forward- and backward-looking interferograms are generated by removing low-frequency signals using the full-aperture interferogram, and they only contain the noise and signal due to the modified squint angle. Using residual interferograms enables us to avoid the unwrapping errors in areas that have a large phase gradient (Sandwell and Price 1998). More details on the use of residual sub-aperture interferograms are given in Sect. 2.3.

In addition, we propose to simplify the processing of MtMAI stacks by creating two independent stacks of forward- and backward-looking interferograms before subtraction of two stacks to form a final MAI interferogram.

This robust time-saving procedure implements the MAI-generation step only once.

We, therefore, propose an approach for stacking multi-temporal MAI interferograms in which the residual forward- and backward-looking interferograms are stacked independently before being combined to create an MAI interferogram:

$$v_{\mathrm{MAI}}(x) = \frac{l}{4\pi \cdot n} \cdot \left[\left\{ \sum_{i=1}^{N} \phi^{i}_{f.\mathrm{res}}(x) \right\} - \left\{ \sum_{i=1}^{N} \phi^{i}_{b.\mathrm{res}}(x) \right\} \right] \Big/ \sum_{i=1}^{N} \Delta t^{i}, \tag{5}$$

where $\phi^{i}_{f.\mathrm{res}}$ and $\phi^{i}_{b.\mathrm{res}}$ are the interferometric phase of ith residual forward- and backward-looking interferograms, respectively.

The theoretical errors in multi-stacked MAI observations are represented using Eq. (5). Assuming that individual MAI interferograms are statistically independent, stacking interferograms should theoretically reduce the noise by a factor of $1/\sqrt{N}$ for independent interferograms relative to one another (Strozzi et al. 2001). As a result, the predicted estimation error $\sigma_{v,\mathrm{MAI}}$ introduced by MAI stacking can be represented by Bechor and Zebker (2006) and Strozzi et al. (2001):

$$\sigma_{v,\mathrm{MAI}} = \frac{l}{4\pi \cdot n} \frac{\sqrt{N} \cdot \sigma_{\phi,\mathrm{MAI}}}{\sum_{i=1}^{N} \Delta t^{i}}, \tag{6}$$

where $\sigma_{\varphi,\mathrm{MAI}}$ is the phase standard deviation of a single MAI interferogram that is defined in Eq. (2). If the time durations of all interferograms are exactly identical, the term $\sqrt{N}/\sum_{i=1}^{N} \Delta t^{i}$ can be rewritten as $1/(\sqrt{N} \cdot \Delta t)$, which indicates that the estimation error is reduced by a factor of $1/\sqrt{N}$. In practical terms, $\sigma_{\varphi,\mathrm{MAI}}$ can be calculated from the mean coherence value of all MAI interferograms because the coherence values of all interferograms may be different with respect to one another.

2.3 Data processing for the proposed MAI stacking

We introduce the processing procedure for the proposed MtMAI stacking method in this section. The method aims to maximize the coherence of MAI by reducing the forward- and backward-looking InSAR phase noise, thereby improving MAI measurement accuracy. The main steps of MtMAI are summarized as follows:

1. Generation of stacked residual forward- and backward-looking interferograms.
2. Generation of the stacked MAI interferogram from the stacked forward- and backward-looking interferograms.
3. Correction of residual phase distortion induced by baseline differences between forward- and backward-looking interferograms (Jung et al. 2009).

The detailed processing procedure of MtMAI from SLC images to final MAI interferogram is the following as shown in Fig. 2. In the first step, a total of four sub-aperture images (two forward- and two backward-looking SLC images from two raw SAR scenes) are generated from the SAR raw signals by modifying the Doppler Centroid on the azimuth spectra of the master and slave acquisitions. Full-aperture master and slave images with average Doppler Centroid are also generated for constructing residual forward- and backward-looking interferograms. This step is an azimuth common-band filtering for improving coherence as well as computation efficiency (Jung et al. 2009). The sizes of sub- and full-aperture SLC images from the same raw data are identical. The details of the Doppler Centroid and bandwidth of sub- and full-aperture SLC images are described in Jung et al. (2009). After preparing the SLC images, forward- and backward-looking interferograms are generated from those data. During this step, multilooking of the sub-aperture interferograms is carried out in the range and azimuth directions to reduce the phase noise of each interferogram. To remove the

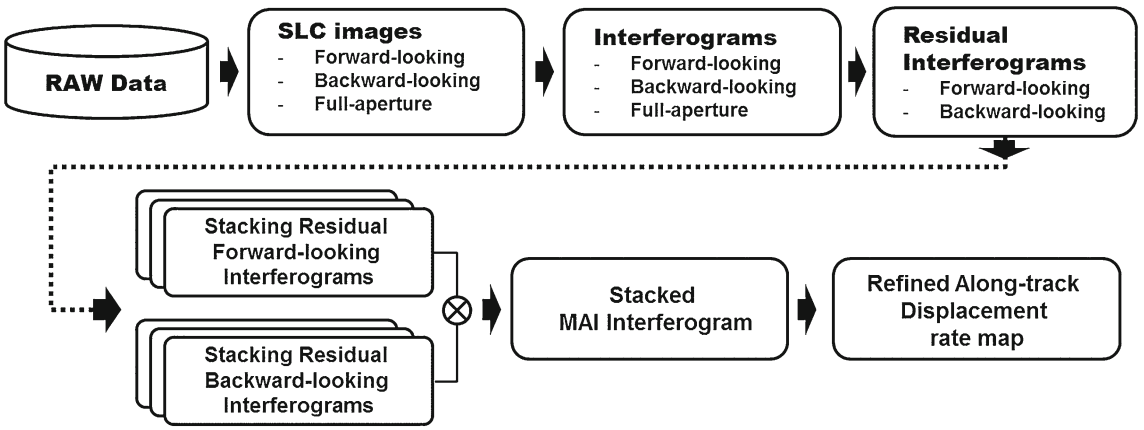

Fig. 2 Diagram for the processing procedure of the proposed MAI stacking method

topographic phase, a digital elevation model derived from 3-second Shuttle Radar Topography Mission (SRTM) data was used to simulate the topographic phase contribution in the InSAR geometry and was subtracted from the interferograms. A full-aperture interferogram is generated in the same way. In this study, single-look-complex images and interferograms were generated using the GAMMA Modular SAR Processor from Gamma Remote Sensing in Switzerland. All processing steps from raw data to MAI interferogram are performed in the radar coordinate system using complex-format data. After generating a final MAI interferogram, that image is unwrapped using a minimum cost flow (MCF) algorithm by Costantini (1998) and transformed to a geographic coordinate system.

The key steps of the MtMAI procedure are generation of residual forward- and backward-looking interferograms, which are formed by removing the phase of the full-aperture interferogram from the phases of the sub-aperture interferograms, and individual stacking of forward- and backward-looking interferograms by multiplication of the complex-formatted residual interferograms. The sub-aperture interferograms and full aperture interferogram have similar phase patterns due to the overlapping signals, especially the topographic phase. In the residual forward- and backward-looking interferograms, therefore, remaining signals represent important surface motion data since the other phase components have been removed. For generation of the residual sub-aperture interferograms, phase filtering of the full-aperture interferogram by Goldstein and Werner (1998) is performed three times with a progressively decreasing window size (from 128 to 64 to 32 pixels). The filtered full-aperture interferogram contains only low-frequency signal with minimal noise and was used to create residual forward- and backward-looking interferograms. A second multilooking was then performed on the residual forward- and backward-looking interferograms.

Individual stacking of forward- and backward-looking interferograms is a noteworthy step of the processing procedure. This step will not only emphasize the surface displacement by reducing unwanted noise, but will also simplify the stacking procedure by implementing the unwrapping process only once.

In the final step, a stacked MAI interferogram is obtained by complex conjugate multiplication of stacked forward- and backward-looking interferograms. This MAI interferogram, however, contains phase distortions due to flat-Earth and topographic effects that are induced by baseline differences between the forward- and backward-looking interferograms. The baselines of the forward- or backward-looking interferograms in stacked states are average values of all the forward- or backward-looking interferograms used for the stacking process. Correction of residual phase distortion was carried out by using the method in Jung et al. (2009).

3 Application and results

3.1 Measurement of along-track displacement

The proposed MAI stacking algorithm was applied to measure surface displacements at Kīlauea Volcano, on the Island of Hawai'i (Fig. 3). Kīlauea is one of the most active volcanoes in the world, with a fluctuating supply of magma from a mantle plume feeding two eruptions—one along the volcano's East Rift Zone (active since 1983) and another at the summit (ongoing since 2008) (Poland et al. 2012). Monitoring surface displacement at Kīlauea is critical for inferring characteristics of magma supply, storage, and transport. As shown in Fig. 3, surface motion at Kīlauea occurs at the summit, along the East and Southwest Rift Zones (ERZ and SWRZ, respectively), and on the south flank. While transient displacement of the summit and rift zones is often related to magmatic intrusions and eruptions, displacement of the south flank is due to creep along a basal décollement fault and is punctuated by discrete, quasi-regular slow-slip events (Montgomery-Brown et al. 2009, 2010).

To test the performance of the proposed MAI stacking method, we used two tracks of ENVISAT ASAR data, including 11 acquisitions from a descending orbit (track 429) and 10 acquisitions from an ascending orbit (track 93). Both tracks cover almost the same time period, from July 2007 to October 2010. During this period, displacement of Kīlauea was characterized by gradual subsidence of the summit and rift zones, as well as steady seaward motion of the south flank [including a slow slip event in 2010 (Poland et al. 2010)]. MAI stacking made use of the raw data from the SAR acquisitions, and topographic effects were removed using SRTM elevation data (Farr et al. 2007). The pixel spacing of the ENVISAT SLC images is approximately 8 m in range and

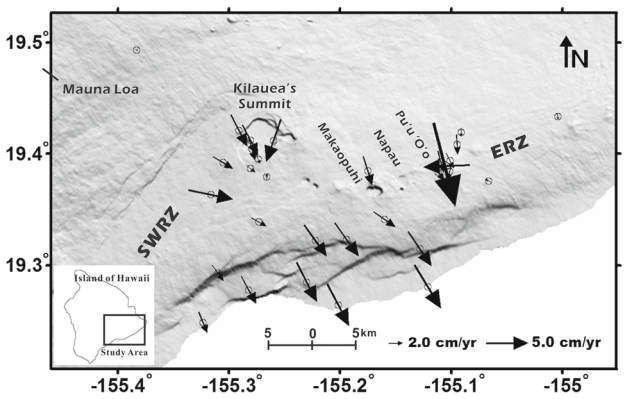

Fig. 3 *Shaded relief map* of Kīlauea and Mauna Loa volcanoes, Hawai'i. *Small open circles* indicate the positions of continuous GPS stations, and *black arrows* represent the magnitudes and directions of horizontal displacements during 2007–2010. *ERZ* East Rift Zone, *SWRZ* Southwest Rift Zone

Table 1 Interferometric pairs of ascending and descending orbit data with perpendicular baselines used in this study

Ascending (path 93)		Descending (path 429)	
Acquisition date	$B_\perp$ (m)	Acquisition date	$B_\perp$ (m)
20070723_20100329	−85	20070711_20100317	127
20070723_20100607	−124	20070711_20100526	10
20071001_20100503	−155	20070711_20100630	139
20071001_20100607	−17	20070711_20100804	−78
20080324_20100329	−117	20080312_20100526	63
20080324_20100607	−156	20080312_20100630	192
20080428_20100329	−54	20080416_20100210	215
20080428_20100607	−93	20080416_20100526	−119
20080811_20100329	−54	20080625_20100210	138
20080811_20100503	−230	20080625_20100526	−197
20080915_20100503	−80	20080730_20100210	134
20090413_20100503	−83	20090225_20100210	58

4 m in azimuth. Multilooking factors of MAI interferograms are 4 and 20 in the range and azimuth directions, respectively. A total of 12 interferograms, chosen to minimize perpendicular baselines, were generated for each track. All the interferometric pairs used for this study are listed in Table 1. Most of the perpendicular baselines are less than 100 m, and the maximum value was limited to 230 m for both ascending and descending tracks. Temporal baselines reach up to 3 years to amplify the surface displacements. An along-track displacement-rate map generated by conventional stacking of separate MAI interferograms was also completed for comparison against the new stacking method.

GPS time-series for 36 stations on Kīlauea (Fig. 3) during 2007–2010 were collected to evaluate the performance of proposed MAI stacking method. The GPS data were corrected for Pacific Plate motion by subtracting the horizontal displacements from a site on Mauna Kea, where no volcanic deformation is occurring, and the along-track component of surface motion was calculated from the east and north components of the GPS displacements. Only GPS stations located in areas where coherence in the MAI interferogram was 0.7 or greater were used for the comparison.

Figure 4a, b shows the along-track displacement-rate maps generated from descending orbit data using both the conventional (Fig. 4b) and proposed (Fig. 4a) MAI stacking methods. Regions with coherence less than 0.7, including most of the north area of Kīlauea's ERZ, were masked out because low-coherence areas do not provide reliable measurements of surface displacements. Results from the two MAI stacking methods show similar displacement patterns, but noise is noticeably reduced by the proposed stacking method (Fig. 4a), particularly near the low-coherence areas. Unlike the conventional method, clear displacements in opposing directions can be seen at the summit and ERZ of Kīlauea in the results of the proposed method. The displacement patterns are consistent with GPS measurements shown in Fig. 3, as well. At the summit of Kīlauea, along-track surface displacement rates suggest deflation due to negative volume change at depth, while southeast-directed displacements are observed on the south flank of the volcano. Similar to the descending results, along-track displacement-rate maps from ascending data show the improvement from the proposed stacking method (Fig. 4c, d)—noise is noticeably reduced and displacements are clear from the results of the proposed stacking method.

Figure 5 shows the coherence maps of the stacked MAI interferograms estimated by the proposed and conventional stacking methods from boxes A and B of Fig. 4. The coherence maps for the ascending acquisitions are seen in Fig. 5a, c, e, g, and those of the descending acquisitions are shown in Fig. 5b, d, f, h. Since the coherence is a crucial factor controlling the measurement accuracy, the coherence analysis provides valuable information concerning the performance of the proposed method. Box A is the summit of Kilauea volcano (Fig. 5a–d) and box B is the lava flow field extending south from Pu'u 'Ō'ō Crater (Fig. 5e–h). These areas were selected to show the large difference between the two stacking methods. The coherence maps from the proposed method preserve high coherence values around Kilauea Caldera (Fig. 5a, b) and the lava flow field (Fig. 5e, f), while those from the conventional method have lower coherence values (Fig. 5c, d, g, h). These results demonstrate the remarkable improvement in measurement accuracy of the MAI velocities at those areas compared to the conventional method (see the boxes A and B of Fig. 4).

Figure 6 shows the coherence histograms of MAI interferograms generated by four types of the different stacking approaches, allowing for a more quantitative identification of coherence improvement. As shown in Fig. 6, similar results were obtained from both the ascending (Fig. 6a) and descending (Fig. 6b) interferometric pairs. Most histograms show a bi-modal distribution, except for the results that were not filtered or multi-looked. The peaks of the coherence histograms close to 1 come from the SWRZ and south flank region because those areas showed the coherent signals from both the conventional and proposed methods. The large differences among the histograms are due to secondary peaks, which are derived from low-coherence regions. The second peak in the proposed stacking method is close to about 0.7—much higher than those of other methods (see Fig. 6). The higher coherence indicates that the proposed method improves the measurement accuracy of the along-track displacements. In addition, if the residual images are not used in the proposed MAI stacking, the coherence histogram is very similar to the conventional stacking method as shown in Fig. 6a, b. The two methods have secondary peaks with coherence values of about 0.3. If the phase fil-

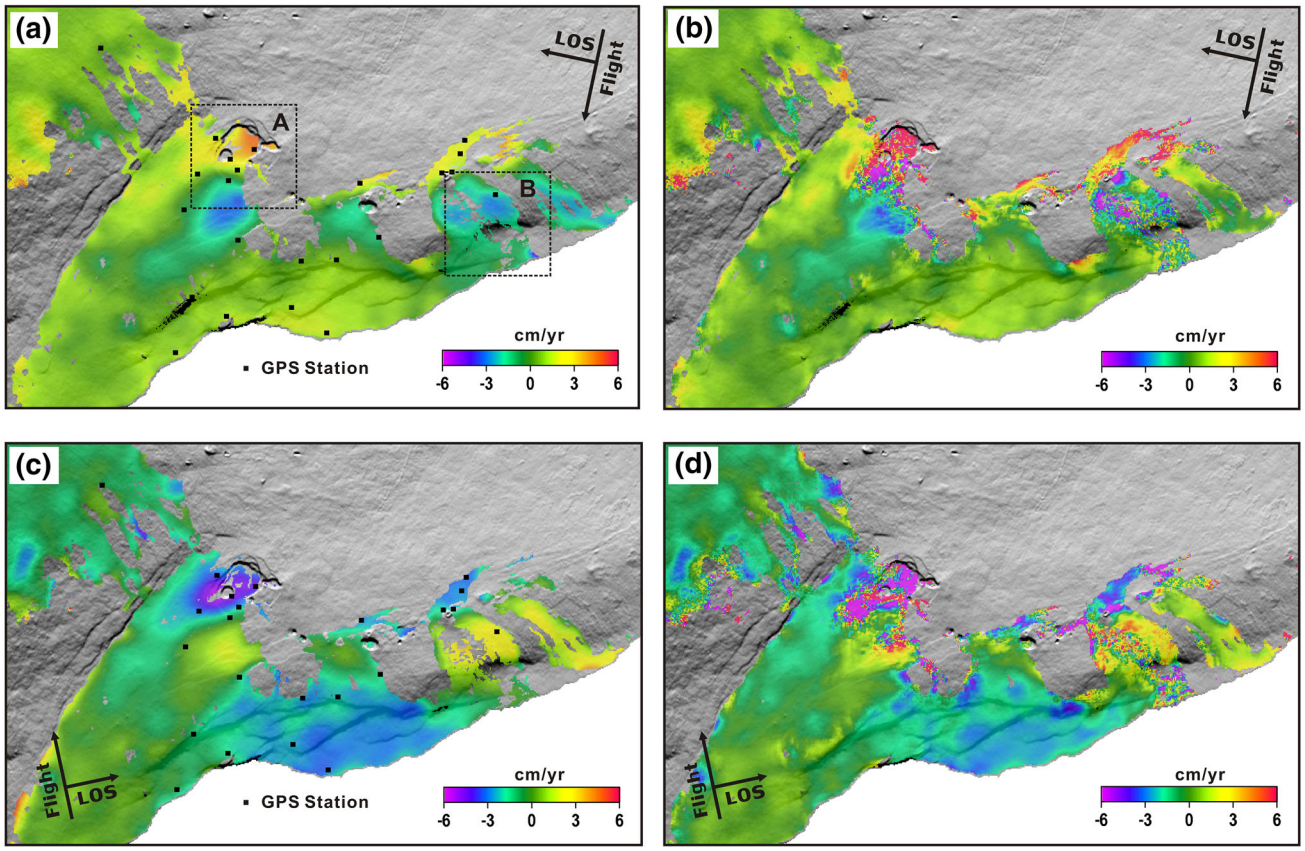

Fig. 4 Comparison between the results of the proposed and conventional MAI stacking methods using ENVISAT ASAR data obtained from descending track 429 and ascending track 93, both beam mode 2 and spanning July 2007–August 2010. **a**, **c** Along-track displacement-rate maps at Kīlauea were generated using the proposed stacking method from tracks 429 and 93, and **b**, **d** the conventional method from tracks 429 and 93. Regions with coherence less than 0.7 were masked (*gray areas*). *The arrows in the corners of the maps* indicate the flight and line-of-sight (LOS) direction of the satellite. *Colors* indicate movements toward (positive values) or away from (negative values) the flight direction. GPS stations used in this study are displayed as small points. *The dashed areas*, *A* and *B*, indicate the sub-region showing coherence map in Fig. 5

tering and multi-looking approaches are not applied to the conventional stacking at all, the coherence histograms show normal distributions with a mean of about 0.2 (see Fig. 6). The results demonstrate the effectiveness and importance of the use of residual phase, phase filtering, and multi-looking in the proposed method.

To quantify the measurement accuracy of the proposed stacking method, we compared results with GPS measurements (Fig. 7a). A total of 20 GPS stations were located in areas where coherence was greater than 0.7 in the descending InSAR pair. The result of the proposed MAI stacking method (Fig. 7a) is clearly more consistent with GPS-derived displacements, compared to the displacements calculated from the conventional stacking method (Fig. 7b). The RMS error by the difference between GPS velocities and along-track velocities are 1.03 and 2.08 cm/year for the proposed and conventional methods, respectively (for measurements within 2σ). Remarkably, the estimated accuracy of the proposed method is an improvement of about a factor of two compared to the conventional stacking approach. The accuracy of the conventional stacking method was improved as well when compared to previous studies using a single MAI pair, but substantial variance in along-track velocities makes the measurements unreliable. The error bars for MAI velocities were calculated from the standard deviation of MAI velocities using a window size of 3×3. In Fig. 7a, b, a large decrease of standard deviation is noticeable when comparing the results of the two stacking methods. The mean standard deviations of the measurements by the proposed and conventional methods are 0.17 and 0.66 cm/year, respectively, for descending data, as summarized in Table 2. The proposed method reduced the noise by 25.7 % from the conventional method. Similar to the result of the descending data, the standard deviations of the measurements by the proposed and conventional methods are 0.18 and 0.74 cm/year, respectively, for ascending data. Comparison with data from 20 GPS stations located in regions with coherence greater than 0.7 quantifies the improvement in measurement accuracy (Fig. 8)—RMS error is 1.07 cm/year

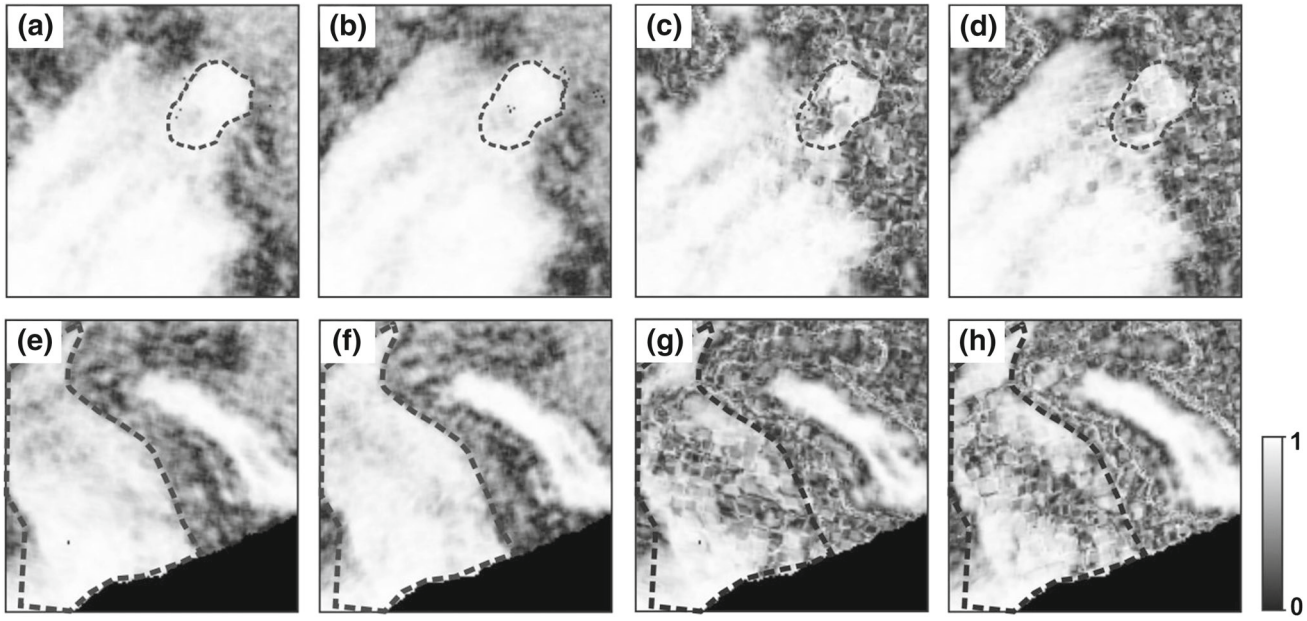

Fig. 5 Coherence maps of stacked MAI interferograms calculated by the proposed and conventional stacking from boxes A and B of Fig. 4: **a**, **b** the proposed and **c**, **d** conventional methods for the ascending and descending acquisitions in box A and **e**, **f** the proposed and **g**, **h** conventional methods for the ascending and descending acquisitions in box B

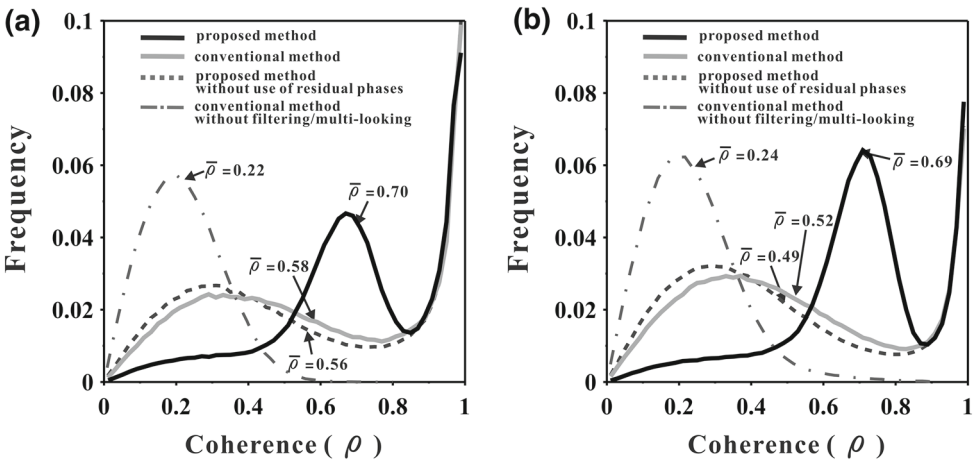

Fig. 6 Comparison between coherence histograms of four types of stacked MAI interferograms for **a** ascending and **b** descending interferometric pairs

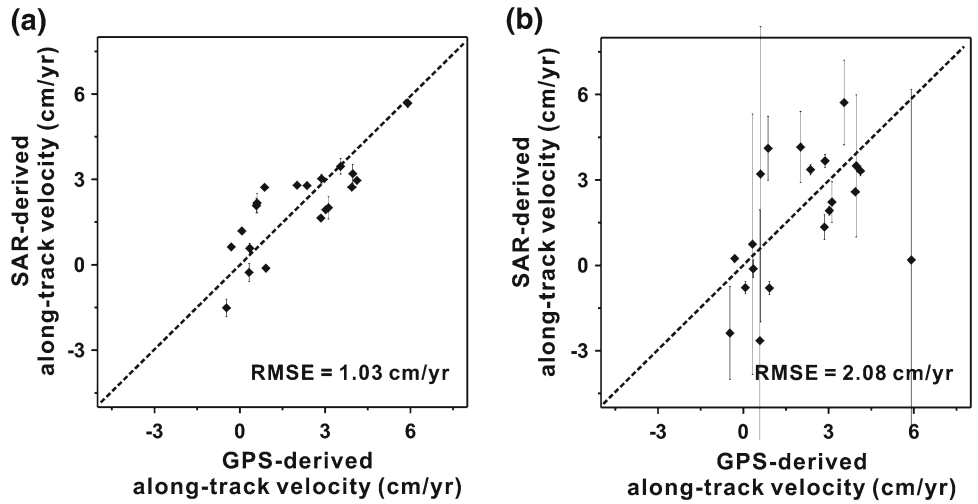

Fig. 7 **a**, **b** Comparison of along-track displacement rates measured from GPS and MAI for the descending track using the proposed method and the conventional method. Twenty GPS sites located in areas with coherence greater than 0.7 were used in the comparison

for the proposed method and 2.13 cm/year for the conventional method (Fig. 8a, b). The accuracies achieved by the proposed and normal stacking method correspond to about 0.2 and 0.41 % of the azimuth resolution of the ENVISAT data, similar to the levels of improvement of the descending data.

The performance test of MAI stacks using two different tracks of ENVISAT data compared to displacements from GPS demonstrates that the proposed stacking method is an effective means of measuring along-track displacement. RMS error for the proposed method is approximately 1.0 cm/year, which is a remarkable improvement over other along-track MAI or SAR pixel offset tracking displacement measurements. We regard this accuracy as reasonable for monitoring slow-moving surface motion in the along-track direction. As with the proposed method, the conventional stacking method shows an improvement when compared to a single observation, but it is difficult to observe slow-moving surface motion due to the low accuracy and large standard deviation of the MAI phase.

In Fig. 9a, b, we display the theoretical errors, estimated using Eq. (6), for the regions with coherence greater than 0.7. The main factor controlling the uncertainty is coherence. In other words, areas showing small uncertainty are regions of high coherence—for instance, on Mauna Loa and on the south flank of Kīlauea. Areas around the ERZ and summit of Kīlauea, on the other hand, show higher uncertainties than other regions due to the loss of coherence induced by the presence of vegetation and rapid, large-magnitude surface displacements. We compared the theoretical uncertainties and GPS-MAI residuals for both tracks of ENVISAT data (see Fig. 9c, d). For the proposed stacking method, the measured GPS-MAI residuals are smaller than the theoretical errors at most GPS sites. In addition, 40 % of the GPS sites show GPS-MAI residuals of less than 1 cm/year in the descending data, and about 70 % of the GPS sites meet this criterion in the ascending data. The primary reason for the smaller GPS-MAI residuals compared to theoretical uncertainty is phase filtering of the interferograms, which is not taken into account by the error calculation in Eq. (6).

Table 2 Standard deviation and RMSE of along-track displacements measured from the proposed and conventional MAI stacking methods

Data set	Proposed method		Conventional method	
	STD (cm/year)	RMSE (cm/year)	STD (cm/year)	RMSE (cm/year)
Descending path	0.17	1.03	0.66	2.08
Ascending path	0.18	1.07	0.74	2.13

3.2 Efficiency test for the proposed MAI stacking

To determine the effective number of MAI interferograms needed for the proposed MAI stacking process, an assessment test for the improvement of coherence and measurement accuracy according to the number of MAI interferograms used for the stacking was completed. Results are compared to those obtained from the conventional stacking method. In this performance test, the number of MAI interferograms used for the stacking is increased from two to eleven pairs. At each stacking step, MAI interferograms are randomly sampled and stacked. This procedure is iterated twelve times for the ascending and descending data, generating a total of twenty-four stacked MAI interferograms. Twenty-four coherence maps are created from the stacked MAI interferograms and used to calculate the mean and standard deviation of coherence values at each stacking step. The value and error bar in the graph of coherence versus number of stacked MAI interferograms (Figs. 10, 11) indicates the mean and standard deviation calculated from the twenty-four coherence maps in each stacking step.

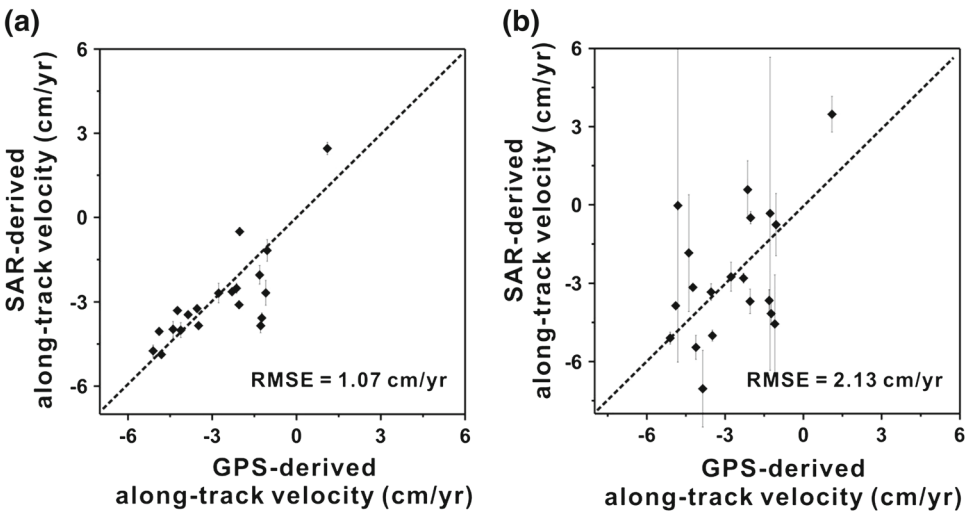

Fig. 8 **a**, **b** Comparison of along-track displacement rates measured from GPS and MAI for the ascending track using the proposed method and the conventional method. Twenty GPS sites located in areas with coherence greater than 0.7 were used in the comparison

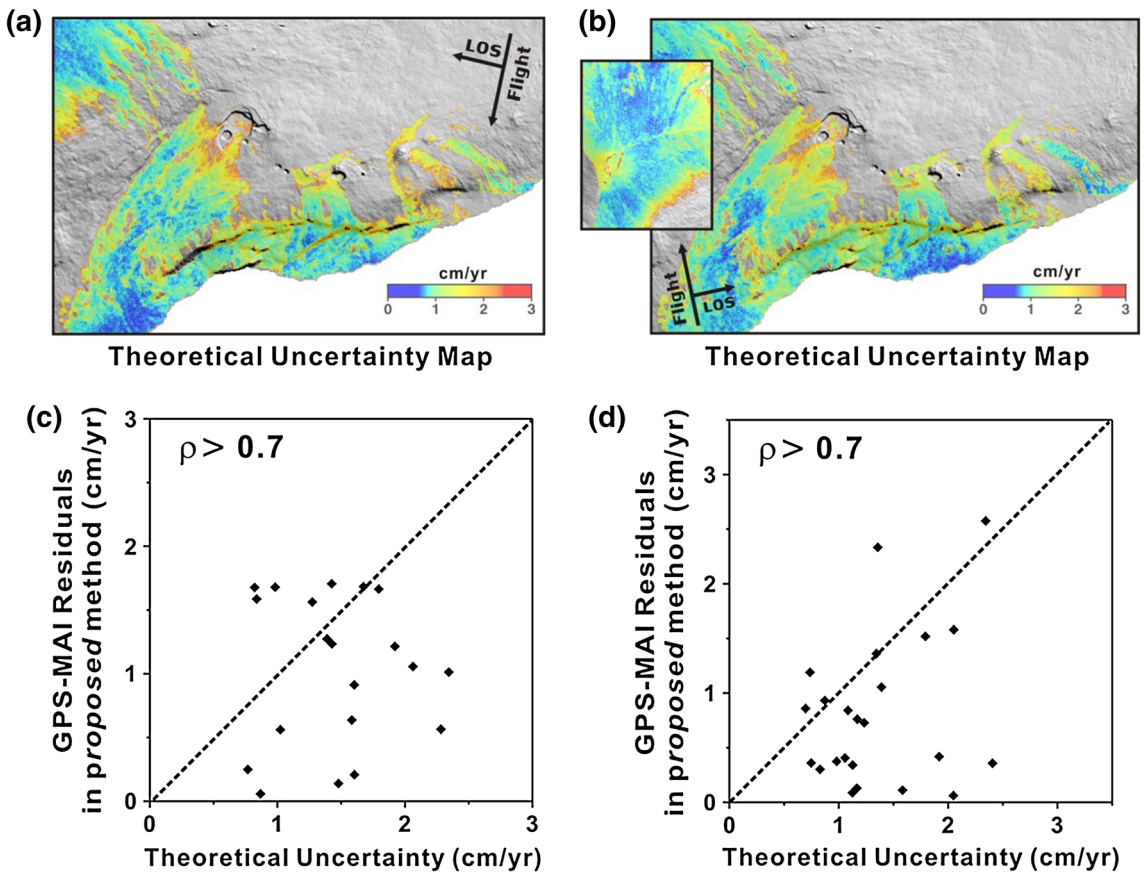

Fig. 9 Comparison between theoretical uncertainties and measured GPS-MAI residuals. **a**, **b** *The first row* gives theoretical uncertainty maps calculated from multi-temporal MAI observations using Eq. (6) for **a** descending and **b** ascending data sets. Smaller uncertainty values indicate regions of higher coherence. *Graphs* show comparison between theoretical uncertainties and measured GPS-MAI residuals. **c**, **d** *The second row* gives the measured GPS-MAI residuals for the proposed method from descending and ascending data sets. Only GPS sites located in areas with coherence greater than 0.7 ($\rho > 0.7$) were used in the analysis

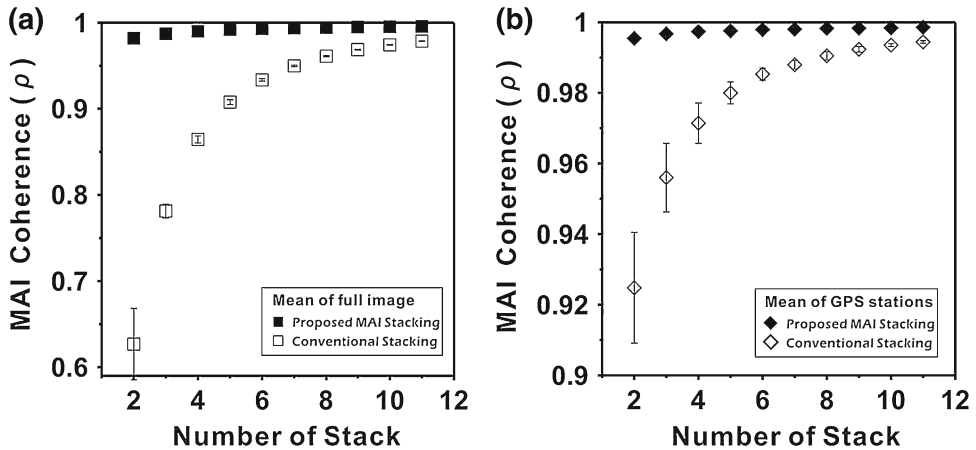

Fig. 10 Comparison of MAI coherence according to the number of stacks between the proposed method (*filled squares* and *diamonds*) and the conventional method (*open squares* and *diamonds*). *The graphs* show **a** the mean coherence of the entire region and **b** the averaged coherence at GPS stations. In **a**, the coherence of the MAI reaches a stable level (about 0.99) after a MAI stacking of 5 images by the proposed method, while even a 12-image stack by the conventional method do not improve coherence to this level

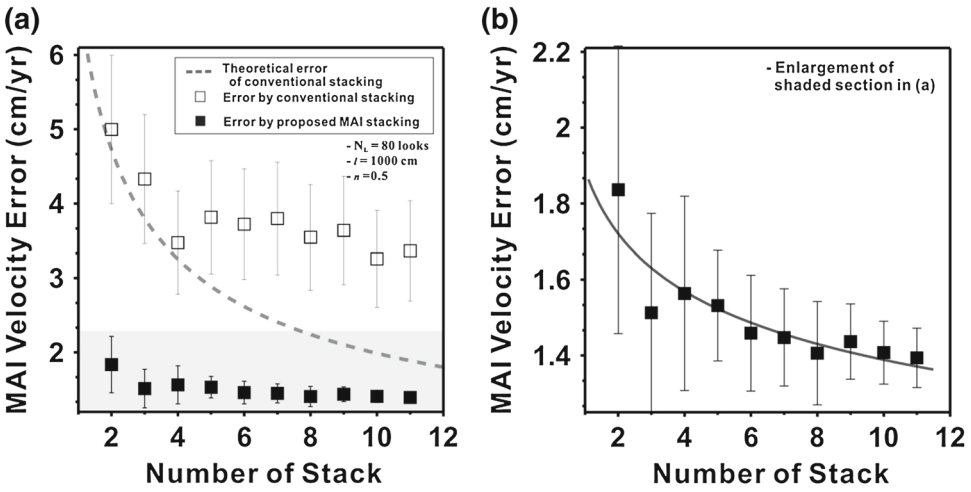

Fig. 11 **a** Comparison of measurement accuracy according to the number of images stacked between the proposed method (*filled squares*) and the conventional method (*open squares*). **b** Enlargement of the proposed MAI stacking section (*shaded region*) in graph **a**. The proposed MAI stacking is superior to the conventional method in terms of measurement error and coherence, and the measurement error of displacement becomes less than 1.5 cm/year after stacking 6 images

Figure 10a, b shows the improvement in coherence for the stacked MAI interferogram using the conventional and proposed methods. The squares in Fig. 10a represent the mean coherence calculated from all pixels of the stacked MAI interferograms, while the diamonds in Fig. 10b show the mean value calculated from the pixels at GPS stations. The coherence value was calculated from MAI interferograms that had been multi-looked (4 looks in range and 20 looks in azimuth) and phase-filtered. As shown in the graphs (Fig. 10), the coherence improvement by the two stacking methods shows a substantial difference. The open squares corresponding to the conventional stacking in Fig. 10a were not able to reach a coherence value of 0.9 until five MAI interferograms are stacked, although the coherence is steadily improved as the number of MAI interferograms is increased. The filled squares calculated from the proposed MAI stacking method, on the contrary, reach high coherence much faster than those of the conventional stacking method, presumably because filtering and multi-looking to sub-aperture interferograms before generating an MAI interferogram lead to significant improvement in MAI coherence, as demonstrated by Jung et al. (2009). The use of residual sub-aperture interferograms also plays a role in this improvement.

The coherence values in Fig. 10b estimated at the GPS station locations show higher levels than those of the entire region from both conventional and the proposed MAI stacking because GPS stations are generally located in areas of low vegetative cover that tend to be very coherent. It can be seen that the coherence by the conventional stacking reaches the level of the proposed MAI stacking when a large number of images are stacked, while there is a notable difference in coherence between two methods when a small number of images are stacked. The difference in coherence between the two stacking methods is less than 0.01 when 10 pairs are stacked. This slight difference, however, corresponds to a measurement error of about 1.0 cm based on Eqs. (2) and (3). The difference becomes larger when the number of available stacks decreases. One can expect to obtain the measurement accuracy about 2.0 and 1.0 cm/year by the conventional stacking and proposed MAI stacking, respectively, from the coherence values of GPS stations when stacking over 10 pairs.

Figure 11a shows the variations in MAI displacement errors by the conventional stacking (open squares) and proposed MAI stacking (filled squares) according to the number of stacks. Measurement errors were calculated using GPS measurements at 36 stations. As a result of the evaluation, it is clear that there is a substantial difference in the error level between the two stacking methods. The errors from the proposed MAI stacking are less by a factor of two compared with those of the conventional stacking. In addition, the error level of the proposed MAI stacking is below the theoretical calculation, and the difference in the error level is reduced according to the number of stacked data. The proposed MAI stacking method thus achieves efficient results for stacking even with a small number of pairs. Figure 11b is an enlargement of the measurement errors for the shaded part in Fig. 11a. As shown in the plot, a decrease of displacement errors relative to the GPS measurements is recognized until 6–7 pairs are stacked by the proposed MAI stacking, but stacking more than 8 pairs does not lead to further improvement in terms of measurement accuracy. The standard deviation, on the other hand, continuously improves with an increasing number of stacks. The minimum error level by the proposed MAI stacking is about 1.4 cm/year when stacking about 10 pairs.

The dashed line in Fig. 11a represents the theoretical error of the stacked MAI interferogram calculated from Eq. (6). The slope of the variation decreases with an increased the number of stacks. The measurement errors from conventional stacking generally follow the theoretical errors until only a few MAI interferograms are stacked. However, similar to the proposed MAI stacking, the errors are no longer reduced by the conventional stacking process after reaching an error level of about 3.5 cm/year.

We presume that the stabilization of the error reduction for the conventional and proposed MAI stacking methods are mainly due to the dependence between interferometric pairs that include the same master or slave images. In an ideal case, there should be no dependence between individual images to suppress randomly distributed noise. The total number of SAR data used for this performance test is, however, only 11 and 10 scenes from descending and ascending orbits, respectively; thus, measurement error may not be minimized because SLC images are used repeatedly when more than five or six interferograms are stacked. Despite this restriction, the proposed MAI stacking shows an acceptable level of accuracy about 1.5 cm/year or less even when comparatively few interferograms are stacked. The proposed MAI stacking method, therefore, is effective for measuring slow-moving displacements in the along-track direction.

3.3 Determination of 3-D displacements

Following previous studies (Wright et al. 2004; Jung et al. 2011), we generated three-dimensional (3-D) displacement-rate maps by combining multi-stacked InSAR and MAI displacements from ascending and descending orbits (Fig. 12). We have two multi-stacked InSAR and MAI observations that we use to determine the east (u_e), north (u_n), and up (u_u) components of surface displacement velocities. The measured LOS displacement d_{los} can be decomposed to the satellite look vector (Fialko et al. 2001):

$$[u_n \sin\phi - u_e \cos\phi] \sin\theta + u_u \cos\theta = d_{los}, \quad (7)$$

where ϕ is the satellite's track angle (measured from the north) and θ is the radar incidence angle at the scattering point. The measured along-track displacement d_{MAI} is represented as

$$u_n \cos\phi + u_e \sin\phi = d_{MAI}. \quad (8)$$

Since we have only two observation values (from ascending and descending orbits) for Eq. (7), 3-D displacement components cannot be obtained due to a rank deficiency. We, therefore, first calculated the north component of 3-D displacement using Eq. (8) with multi-stacked MAI displacements. The solution we obtain for the north component replaces the unknown in Eq. (7). This inversion method is slightly different than the general method, but might produce

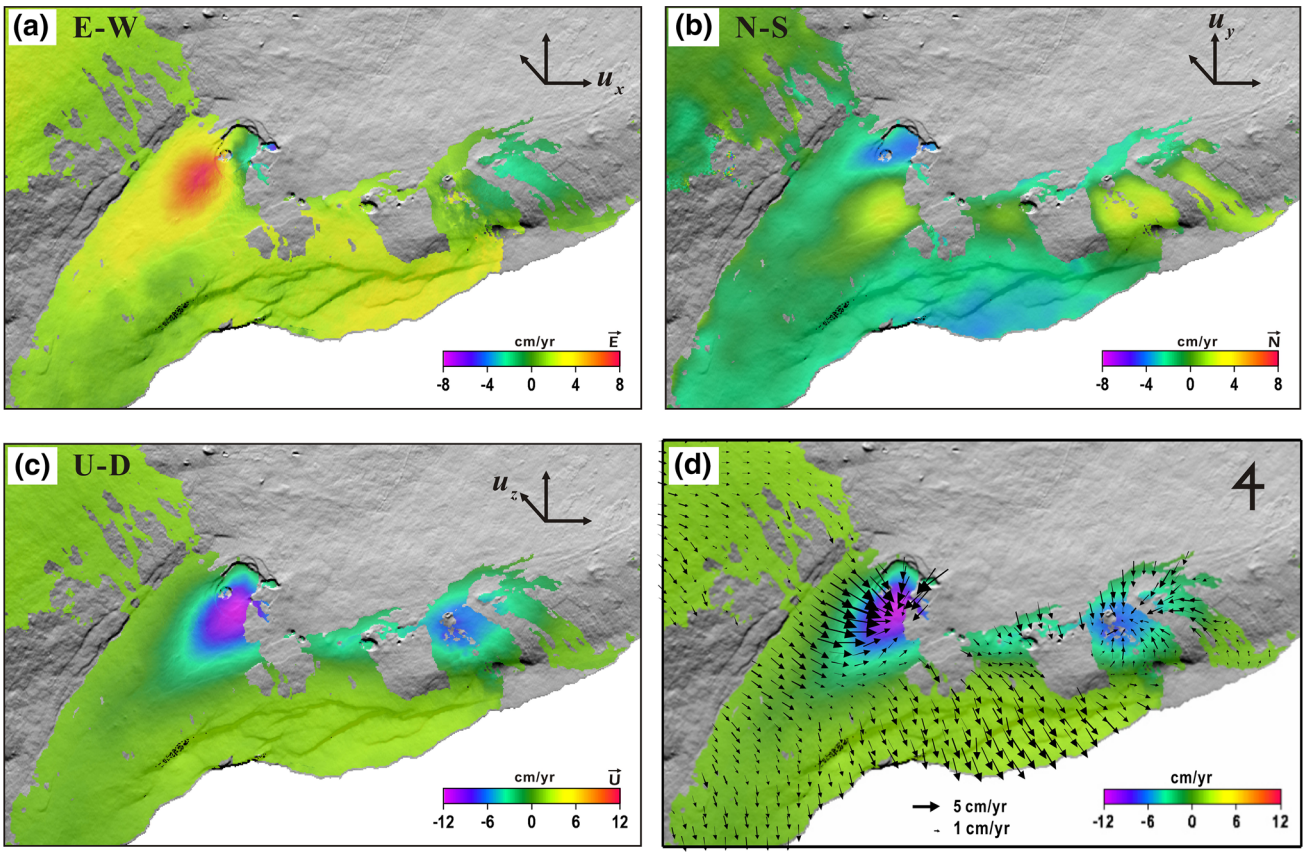

Fig. 12 3-D surface-displacement maps derived from combining multi-stacked InSAR and MAI displacements from ascending and descending orbits: **a** east, **b** north, and **c** up components of 3-D displacement. **d** 3-D surface displacement field, with *arrows* indicating the horizontal displacements and *colors* representing the vertical displacements

the better results, particularly because the MAI measurement does not contain atmospheric effects due to the cancellation between forward- and backward-looking interferograms. On the contrary, the LOS observation can retain atmospheric phase contributions even when stacked. To retrieve the 3-D components, therefore, we can expect better results by the use of north component calculated from MAI observations (by using Eq. 8). The east and up components, however, are primarily dependent on traditional InSAR observations.

At the summit of Kīlauea, motion consistent with deflation is observed in both the east (Fig. 12a) and north (Fig. 12b) components. Similarly, deflation of the Pu‘u ‘Ō‘ō region on the volcano's ERZ is indicated from the 3-D component maps. At the subsiding regions, horizontal displacements approaching to the center of deflation from all directions are common, and deflation of the summit and Pu‘u ‘Ō‘ō is clearly indicated by downward vertical displacements (Fig. 12c). From the patterns of 3-D surface-displacement-rate maps, the locus of deflation is not located exactly in the center of the caldera, but rather on its south side, consistent with previous results by Poland et al. (2012). Figure 12d shows the 3-D displacement-rate field, with horizontal motion indicated by arrows and vertical motion by colors. Surface displacement velocities of specific points on the summit and south flank of Kīlauea estimated by GPS and SAR data are summarized in Table 3.

Figure 13 shows a comparison between GPS measurements and 3-D surface-displacement velocities derived from combined MAI and InSAR observations. A total of 20 GPS stations are used for calculating RMS errors. As demonstrated in Fig. 13a, the east component shows excellent agreement between the two measurement methods because it is mostly dependent on LOS displacements, which have better precision than along-track displacements measured from MAI. However, the measurement from the CNPK station which is located on the southwest limb of the Kilauea's summit showed abnormal measurement (open symbol) from Fig. 13a. Excluding this outlier, estimated RMS error between GPS and SAR measurements in the east component is 0.69 cm/year (1.22 cm/year is obtained when the outlier is included). The up component of displacement is obtained mostly from LOS displacement as well. The estimated RMS error of the up component is 1.40 cm/year when three outliers (open symbols) located at the summit of Kīlauea were not included. The large difference in GPS and 3-D-derived east and up components at some stations is a result of overestimation of LOS displacement at the summit of Kīlauea. We are not sure of the reason for the abnormal phase delay of InSAR measurements at the summit area, but we suspect that water vapor in the atmosphere plays a role (Rosen et al. 1996). The relatively large RMS error of the up component when compared to east component is due to the poorer precision of the vertical GPS data (compared to the horizontal). The RMS error of 0.88 cm/year in the north component is smaller than that of the individual ascending and descending data (Fig. 13b). The north component is mainly determined from MAI observations; therefore, combining ascending and descending data reduces the noise level and improves the accuracy.

By generating a 3-D surface-displacement-rate map, we confirmed that the accuracy range of east, north, and up components derived from combined InSAR and MAI observations is sufficient to measure slow-moving surface displacement. Compared with a previous study of 3-D displacement by Jung et al. (2011), our results achieve an improvement of more than factor of two. The accuracy of the north component, in particular, shows remarkable improvement compared with previous studies—more than four times. The improved performance in surface-displacement monitoring using SAR and combining InSAR and MAI methods should provide important observations for modeling both high- and low-rate surface displacements associated with a variety of geologic processes.

4 Conclusions

We have proposed an efficient stacking method for measuring surface displacements derived from MAI. The core of the proposed stacking method is that multi-temporal forward- and backward-looking interferograms are stacked as residual phases, which are created by removing low-frequency signals from sub-aperture interferograms. In addition, forward- and backward-looking interferograms are individually stacked before MAI creation to maximize the interferometric coherence and emphasize the deformation signals. To evaluate the performance of the proposed MAI stacking method, GPS- and SAR-derived along-track displacements from Kīlauea Volcano, Hawai‘i, were compared. The accuracies of the proposed method, estimated from descending and ascending data, are, respectively, about 1.03 and 1.07 cm/year—about a six-time decrease in root-mean-square error compared to pre-

Table 3 Surface displacement velocities of the summit and the south flank region of Kīlauea Volcano estimated from GPS and SAR observations

Displacement area	GPS velocity (cm/year)			SAR velocity (cm/year)		
	u_x	u_y	u_z	u_x	u_y	u_z
Summit of Kilauea	1.49	−2.18	−4.25	1.50	−2.63	−4.92
South flank	2.10	−3.48	0.35	2.06	−3.31	0.64

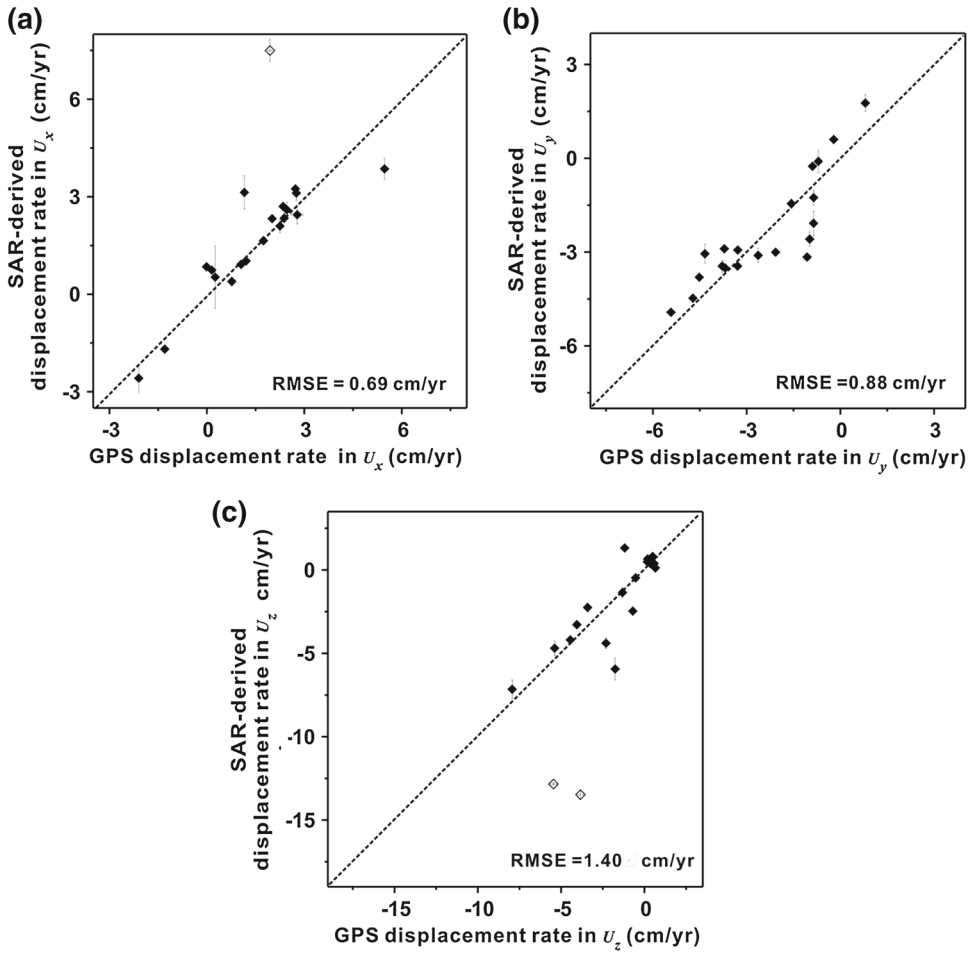

Fig. 13 Comparison between GPS and 3-D surface displacements derived from MAI and InSAR observations using data from 20 GPS stations that are located in areas where coherence was greater than 0.7: **a** east, **b** north, and **c** up components. *Open symbols* indicate outliers from stations that are located in the summit area of Kīlauea Volcano and that are not included when estimating RMS error

vious studies—a noteworthy improvement in the respective accuracies of about 2.08 and 2.13 cm/year for the conventional MAI stacking method. This error range is appropriate for monitoring slow-moving surface motion in the along-track direction. We also estimated the theoretical uncertainties of multi-temporal MAI observations and compared the results with measured GPS-MAI residuals. For the proposed method, errors determined from GPS-MAI residuals were equal to or smaller than theoretical uncertainties at more than 75 % of the GPS sites.

We generated a 3-D displacement-rate map by combining multi-stacked InSAR and MAI displacements from ascending and descending orbital tracks. A comparison between GPS and 3-D components derived from MAI and InSAR indicated measurement accuracy of 0.69, 0.88, and 1.40 cm/year for the east, north, and up components, respectively—an improvement of more than a factor of two compared with previous studies that derive 3-D displacements from InSAR data.

We conclude that the proposed MAI stacking method can improve the measurement accuracy of along-track displacements to ∼1 cm/year. Combining such results with LOS InSAR data enables the creation of 3-D displacement maps that can provide important constraints on modelling a variety of geologic phenomena.

Further improvement of the MAI technique can be achieved by time-series analysis, such as the permanent scatterer InSAR (PSInSAR) and small baseline subset (SBAS) approaches, which are capable of characterizing nonlinear deformation (stacking can only measure linear deformation rates). Time-series methods can also mitigate ionospheric distortions using spatial low-pass and temporal high-pass filtering. Improved temporal resolution of deformation may be achieved by incorporating Sentinel-1 data into MAI stacking or MAI time-series analysis, given the 6-day repeat provided by the two-satellite constellation, although the azimuth resolution is very low (about 20 m).

Acknowledgments The research described in this paper was carried out with financial support from the Space Core Technology Development Program through the National Research Foundation of Korea, funded by the ministry of education, science and technology (2012M1A3A3A02033465). This study also supported by the MSIP (Ministry of Science, ICT and Future Planning) and NRF (National Research Foundation of Korea) under the Space Core Technology Development Program (project id: 2013M1A3A3A02042314). The Hawai‘i GPS network is supported by grants from the USGS, NSF,

and NASA, and is operated in collaboration by the USGS, Stanford University, and Pacific GPS Facility at the University of Hawai'i. GPS RINEX data are archived at UNAVCO.

References

Amelung F, Yun SH, Walter TR, Segall P, Kim SW (2007) Stress control of deep rift intrusion at Mauna Loa Volcano, Hawaii. Science 316(5827):1026–1030

Bechor NBD, Zebker HA (2006) Measuring two-dimensional movements using a single InSAR pair. Geophys Res Lett 33(L16311). doi:10.1029/2006GL026883

Berardino P, Fornaro G, Lanari R, Sansosti E (2002) A new algorithm for surface deformation monitoring based on small baseline differential SAR interferograms. IEEE Trans Geosci Remote Sens 40(11):2375–2383

Costantini M (1998) A novel phase unwrapping method based on network programming. IEEE Trans Geosci Remote Sens 36(3):813–821

Doin MP, Lasserre C, Peltzer G, Cavalie O, Doubre C (2009) Corrections of stratified tropospheric delays in SAR interferometry: validation with global atmospheric models. J Appl Geophys 69:35–50

Farr TG, Rosen PA, Caro E, Crippen R, Duren R, Hensley S, Kobrick M, Paller M, Rodriguez E, Roth L, Seal E, Shaffer S, Shimada J, Umland J, Werner M, Oskin M, Burbank D, Alsdorf D (2007) The shuttle radar topography mission. Rev Geophys 45:RG2004

Ferretti A, Prati C, Rocca F (2001) Permanent scatterers in SAR interferometry. IEEE Trans Geosci Remote Sens 39:8–20

Fialko Y, Simons M, Agnew D (2001) The complete (3-D) surface displacement field in the epicentral area of the 1999 Mw 7.1 Hector Mine earthquake, California, from space geodetic observations. Geophys Res Lett 28(16):3063–3066

Goldstein RM, Werner CL (1998) Radar interferogram filtering for geophysical applications. Geophys Res Lett 25(21):4035–4038

Hu J, Li ZW, Ding XL, Zhu JJ, Zhang L, Sun Q (2012) 3D coseismic displacement of 2010 Darfield, New Zealand earthquake estimated from multi-aperture InSAR and D-InSAR measurements. J Geod 86:1029–1041

Jo MJ, Won JS, Kim SW, Jung HS (2010) A time-series SAR observation of surface deformation at the southern end of the San Andreas Fault Zone. Geosci J 14(3):277–287

Jonsson S, Zebker H, Segall P, Amelung F (2002) Fault slip distribution of the Mw 7.1 Hector Mine, California, earthquake, estimated from satellite radar and GPS measurements. Bull Seismol Soc Am 92(4):1377–1389

Jung HS, Won JS, Kim SW (2009) An improvement of the performance of multiple aperture SAR interferometry (MAI). IEEE Trans Geosci Remote Sens 47(8):2859–2869

Jung HS, Lu Z, Won JS, Poland MP, Miklius A (2011) Mapping three-dimensional surface deformation by combining multiple-aperture interferometry and conventional interferometry: application to the June 2007 eruption of Kilauea volcano, Hawaii. IEEE Geosci Remote Sens Lett 8(1):34–38

Jung HS, Lee DT, Lu Z, Won JS (2013a) Ionospheric correction of SAR interferograms by multiple-aperture interferometry. IEEE Trans Geosci Remote Sens 51(5):3191–3199

Jung HS, Lu Z, Zhang L (2013b) Feasibility of along-track displacement measurement from Sentinel-1 interferometric wide-swath mode. IEEE Trans Geosci Remote Sens 51(1):573–578

Liu Z, Jung HS, Lu Z (2014) Joint correction of ionosphere noise and orbital error in L-band SAR interferometry of interseismic deformation in southern California. IEEE Trans Geosci Remote Sens 52(6):3421–3427

Lu Z, Dzurisin D, Biggs J, Wicks C, McNutt S (2010) Ground surface deformation patterns, magma supply, and magma storage at Okmok volcano, Alaska, from InSAR analysis: 1. Intereruption deformation, 1997–2008. J Geophys Res 115:B00B02. doi:10.1029/2009JB006969

Lyons S, Sandwell D (2003) Fault creep along the southern San Andreas from interferometric synthetic aperture radar, permanent scatters, and stacking. J Geophys Res 108(B1). doi:10.1029/2002JB001831

Massonnet D, Rossi M, Carmona C, Adragna F, Peltzer G, Fiegl K, Rabaute T (1993) The displacement field of the Landers earthquake mapped by radar interferometry. Nature 364:138–142

Mcmillan M, Shepherd A, Gourmelen N, Park JW, Nienow P, Rinne E, Leeson A (2012) Mapping ice-shelf flow with interferometric synthetic aperture radar stacking. J Glaciol 58(208):265–277

Montgomery-Brown EK, Segall P, Miklius A (2009) Kilauea slow slip events: identification, source inversions, and relation to seismicity. J Geophys Res 114:B00A03. doi:10.1029/2008JB006074

Montgomery-Brown EK, Sinnett DK, Poland M, Segall P, Orr T, Zebker H, Miklius A (2010) Geodetic evidence for en echelon dike emplacement and concurrent slow slip during the June 2007 intrusion and eruption at Kilauea volcano, Hawaii. J Geophys Res 115:B07405. doi:10.1029/2009JB006658

Poland M, Miklius A, Wilson D, Okubo P, Montgomery-Brown E, Segall P, Brooks B, Foster J, Wolfe C, Syracuse E, Thurber C (2010) Slow slip event at Kilauea Volcano. EOS Trans AGU 91(13):118–119

Poland MP, Miklius A, Sutton AJ, Thornber CR (2012) A mantle-driven surge in magma supply to Kilauea Volcano during 2003–2007. Nat Geosci 5:295–300

Rodriguez E, Martin JM (1992) Theory and design of interferometric synthetic aperture radars. IEE Proc Part F Radar Signal Process 139(2):149–159

Rosen PA, Hensley S, Zebker HA, Webb FH, Fielding EJ (1996) Surface deformation and coherence measurements of Kilauea Volcano, Hawaii, from SIR-C radar interferometry. J Geophys Res 101(E10):23109–23125

Sandwell DT, Price EJ (1998) Phase gradient approach to stacking interferograms. J Geophys Res 103(B12):30183–30204

Sandwell DT, Myer D, Mellors R, Shimada M, Brooks B, Foster J (2008) Accuracy and resolution of ALOS interferometry: vector deformation maps of the Father's Day intrusion at Kilauea. IEEE T Geosci Remote 46(11):3524–3534

Simons M, Rosen PA (2007) Interferometric synthetic aperture radar geodesy. Treatise Geophys 3:391–446

Strozzi T, Wegmuller U, Tosi L, Bittlli G, Spreckels V (2001) Land subsidence monitoring with differential SAR interferometry. Photogramm Eng Remote 67(11):1261–1270

Wright T, Parsons B, Fielding E (2001) Measurement of interseismic strain accumulation across the North Anatolian Fault by satellite radar interferometry. Geophys Res Lett 28(10):2117–2120

Wright TJ, Parsons BE, Lu Z (2004) Toward mapping surface deformation in three dimensions using InSAR. Geophys Res Lett 31:L01607. doi:10.1029/2003GL018827

Zebker HA, Villasenor J (1992) Decorrelation in interferometric radar echoes. IEEE Trans Geosci Remote 30(5):950–959

Zhang L, Lu Z, Ding X, Jung HS, Feng G, Lee CW (2012) Mapping ground surface deformation using temporarily coherent point SAR interferometry: application to Los Angeles Basin. Remote Sens Environ 117:429–439